PNAS
www.pnas.org

Supplementary Information for

Trophic Interactions with Heterotrophic Bacteria Limit the Range of *Prochlorococcus*

C. L. Follett, S. Dutkiewicz, F. Ribalet, E. Zakem, D. Caron, E. V. Armbrust, and M. J. Follows

Correspondence Should be Adressed to
Christopher L. Follett
E-mail: follett@mit.edu

This PDF file includes:

Supporting Information Text

S1. Collapse Explained in Terms of a Continuous Size Spectrum

Instead of focusing on discrete size classes and completing the nutrient flow as in Main Text Fig. 2A, we can approximate the time evolution of the continuous size distribution of a plankton class directly. We write the biomass distribution, $\rho_i(r)$, where r is the organism's size and i its type (like phytoplankton) as

$$\frac{d\rho_i(r)}{dt} = \mu_i \rho_i - m\rho_i^2 \quad [s1]$$

where $\mu_i(r)$ is the growth rate and m the death rate. To simplify the mathematics, we have approximated the effect of zooplankton predation as the nonlinear death rate term, $-m\rho_i^2$. μ is expressed as a Michaelis-Menten equation in terms of the limiting resource, R, maximum growth rate, μ_{max}, and size scaling exponents (α and β)

$$\mu_i \approx \frac{\mu_i^{max} \tilde{R}_i r^{\alpha}}{r^{\beta} + \tilde{R}_i}. \quad [s2]$$

The half-saturation constant κ_i is eliminated by defining $\tilde{R}_i = \frac{R_i}{\kappa_i}$. Combining this equation with the steady state solution for $\rho_i = \frac{\mu_i}{m}$ from Eq s1 provides a simple prediction for the size distribution. As the resource supply (concentration in steady state) increases, the relative abundance of larger size classes increases relative to smaller size classes, but the absolute concentration of the smaller size classes always increases since $\frac{\partial \rho}{\partial R} > 0$. As the concentration of a size class increases, its grazing rate constant also increases providing an opportunity for the grow-in of larger and larger size classes of phototrophs. Similar to the main text, these equations do not allow for the elimination of a phytoplankton size class.

We can explain the crash of *Prochlorococcus* populations poleward by considering the size spectrum of heterotrophic bacteria along with autotrophs. Eq s1 is sufficient for this case, with the addition that we assume zooplankton feed depending on size so that

$$\frac{d\rho_i(r)}{dt} = \mu_i \rho_i - m\left(\sum \rho_i\right)\rho_i. \quad [s3]$$

The summation term represents the fact that the zooplankton population in steady state is proportional to the sum of all plankton types (i) in the size class that they consume. If we allow there to be two plankton types (h for heterotrophic bacteria and p for phytoplankton), we can solve for the organism size, r_c, where phytoplankton outcompete heterotrophic bacteria. We do this by setting $\mu_h = \mu_p$ in steady state and find

$$r_c = \left(\frac{\mu_h^{max} - \mu_\rho^{max}}{\frac{\mu_\rho^{max}}{\tilde{R}_h} - \frac{\mu_h^{max}}{\tilde{R}_\rho}} \right)^{\frac{1}{\beta}}. \quad [s4]$$

The α scaling drops out of the equation, and using (1) we can simplify further by noting that $\beta \approx 1$. This equation suggests that the size transition to autotrophy increases with increasing organic nutrient supply. At a critical production rate, we expect the smallest autotrophs, in this case *Prochlorococcus* to be replaced by heterotrophic bacteria.

Since the organic material, R_h, heterotrophic bacteria feed upon comes from primary production, we can formalize this idea by assuming that a constant fraction of primary production, f, becomes heterotrophic growth. Under this condition

$$\int_0^{r_c} \mu_h^2 = f \int_{r_c}^{\infty} \mu_\rho^2 \quad [s5]$$

and the concentrations match at the critical size, r_c. Since the sensitivity of the growth rate relative to nutrients increases monotonically with size, increasing R_ρ always leads to an increase in r_c: $\frac{dr_c}{dR_\rho} > 0$. Thus, under the assumptions used to generate the theory, at a critical resource supply, r_c becomes large enough to exclude *Prochlorococcus*.

S2. Zero-Dimensional Model

In the experiments in Main Text Fig. 3B,D for simplicity in illustration, we used only an external supply rate (S_{R_p}). That is, the remineralization component was assumed to implicitly be part of the rate provided. In one of the additional experiments (Supplemental Fig. S1C), we instead assume a closed system such that S_{R_p} is only the remineralization of organic matter. Here the different final solutions shown are instead set by the initial total nitrogen (sum of living, detrital and inorganic) in the system. The results are qualitatively similar. In another final experiment (Fig. S1D), we allow the half-saturation constants k_p and k_h to have different exponents (in this case k_h exponent is double that of k_p). Again, though quantitatively different, the results remain qualitatively the same.

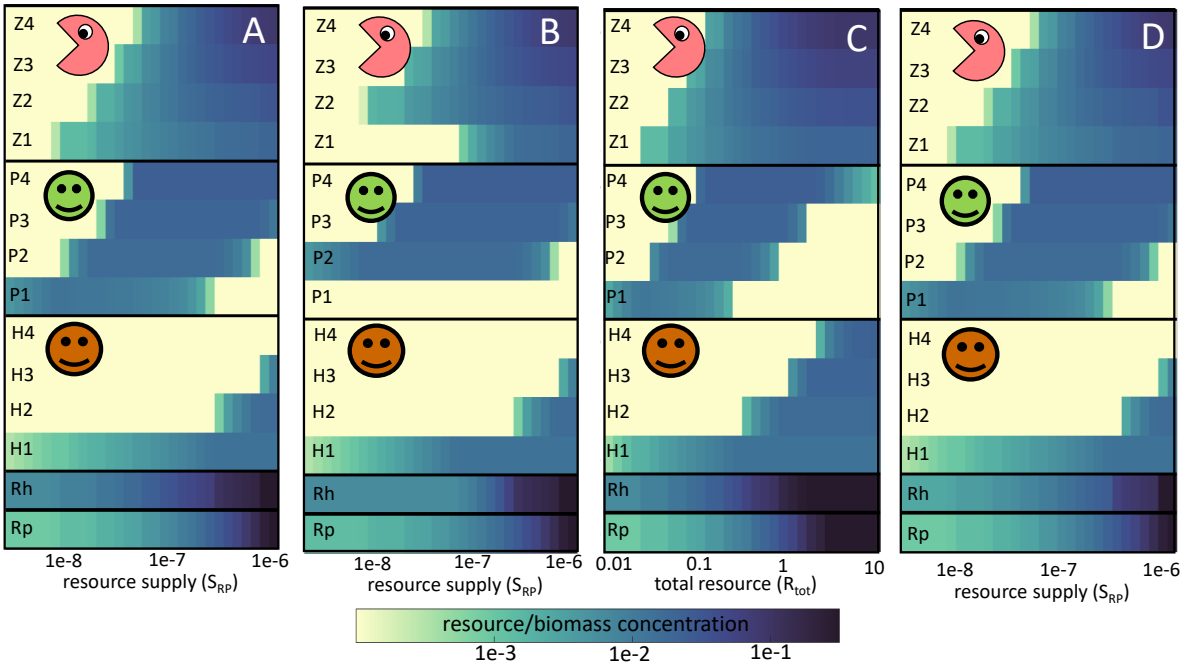

Fig. S1. Solutions for zero-D numerical model with parameter and ecosystem modifications: (A) for original experiment (same plot as in Fig. 3D), (B) same as A but initialized without the smallest phytoplankton size class, (C) solutions found for different total resource rather than for external resource supply; in this example S_{R_p} is just the remineralization component $(1-\delta)\sum \mu_{hj} H_j$, (D) same as (A) but with exponent of half-saturation constant double that given in Supplemental Table S1. Solutions are steady state for low resource supply rates/total resource, and averages over several cycles of predator-prey oscillations that occur for higher resource supply rates/total resource.

S3. Global Biophysical Model

The model we use is based on a previous model (2). Here we outline the differences to that model. We reduce the number of phytoplankton from 35 types to 31 types, removing some of the larger size classes that did not survive in the earlier studies. Missing traits such as buoyancy regulation, shape, spines, or chain formation might have allowed these larger sizes to exist, but such additional components of model development are beyond the scope of this study. We added three heterotrophic bacteria and thus an explicit remineralization loop rather than the rate based parameterization as in our earlier models. We also added a smaller zooplankton class as a grazer for the smallest heterotrophic bacteria. Most parameters are as used in our previous size-based models (2–5). However, given a newer laboratory synthesis paper (6), we use different coefficients for the functional group maximum growth rates (see Table S1), as well as differences in group temperature functions.

References

1. E Litchman, CA Klausmeier, OM Schofield, PG Falkowski, The role of functional traits and trade-offs in structuring phytoplankton communities: Scaling from cellular to ecosystem level. *Ecol. Lett.* **10**, 1170–1181 (2007).
2. S Dutkiewicz, PW Boyd, U Riebesell, Exploring biogeochemical and ecological redundancy in phytoplankton communities in the global ocean. *Glob. Chang. Biol.* **27**, 1196–1213 (2021).
3. S Dutkiewicz, et al., Dimensions of marine phytoplankton diversity. *Biogeosciences* **17**, 609–634 (2020).
4. M Sonnewald, S Dutkiewicz, C Hill, G Forget, Elucidating ecological complexity: Unsupervised learning determines global marine eco-provinces. *Sci. Adv.* **6**, eaay4740 (2020).
5. AM Kuhn, K Fennel, Evaluating ecosystem model complexity for the northwest North Atlantic through surrogate-based optimization. *Ocean. Model.* **142**, 101437 (2019).
6. S Anderson, A Barton, S Clayton, S Dutkiewicz, T Rynearson, Marine phytoplankton functional types exhibit diverse responses to thermal change. *Nat. Commun.* **12**, 6413 (2021).
7. MJ Follows, S Dutkiewicz, B Ward, C Follett, Theoretical interpretations of subtropical plankton biogeography in *Microbial Ecology of the Oceans*, ed. DK Gasol, Josep. (John Wiley & Sons, Ltd, Hoboken, NJ), 3rd edition, p. 467 (2018).
8. BA Ward, Temperature-correlated changes in phytoplankton community structure are restricted to polar waters. *PLoS ONE* **10** (2015).
9. ET Buitenhuis, et al., MAREDAT: Towards a world atlas of MARine Ecosystem DATa. *Earth Syst. Sci. Data* **5**, 227–239 (2013).
10. ET Buitenhuis, et al., Picophytoplankton biomass distribution in the global ocean. *Earth Syst. Sci. Data* **4**, 37–46 (2012).
11. CJ O'Brien, et al., Global marine plankton functional type biomass distributions: Coccolithophores. *Earth Syst. Sci. Data* **5**, 259–276 (2013).
12. YW Luo, et al., Database of diazotrophs in global ocean: Abundance, biomass and nitrogen fixation rates. *Earth Syst. Sci. Data* **4**, 47–73 (2012).
13. K Leblanc, et al., A global diatom database- Abundance, biovolume and biomass in the world ocean. *Earth Syst. Sci. Data* **4**, 149–165 (2012).

parameter		a	b	units
phytoplankton maximum growth rate μ_p^{max}	**0-D model**			1/day
	<3μm	1.1063	0.28	
	>3μm	2.5383	-0.10	
	3-D model			
	pico-cyan	1.1063	0.28	
	pico-euk	1.2066	0.28	
	cocco	1.9454	0.08	
	diazo	0.8083	-0.10	
	diatom	2.5383	-0.10	
	dino	1.3355	-0.10	
hetrotrophic bacteria maximum growth rate μ_h^{max}		1.836	0.28	1/day
nutrient uptake half saturation constant, k	NO_3	0.17	0.27	mmol N/m^3
minimum cell quota, Q^{min}	N	0.07	-0.17	mmol N/ mmol C
maximum nutrient uptake rate, V^{max}	NO_3	0.51	-0.27	
sinking	**0-D model**			m/day
	plankton	0		
	3-D model			
	phytoplankton	0.28	0.39	
	het bacteria	0.28	0.39	
	zooplankton	0		
maximum per capita grazing g	**0-D model** zooplankton	3.63	-0.16	m^3/mmol N/day
maximum grazing rate g^{max}	**3-D model** mixotrophs	12.7	-0.16	1/day
	zooplankton	15.9	-0.16	

Table S1. Allometric parameters used in the two sets of numerical experiments. Parameters values are given aV^b where V is cell volume. Half-saturation constant for growth κ used in the equations in the Monod form are given by the function $\kappa = k\frac{\mu^{max}Q^{min}}{V^{max}}$ following (3, 7).

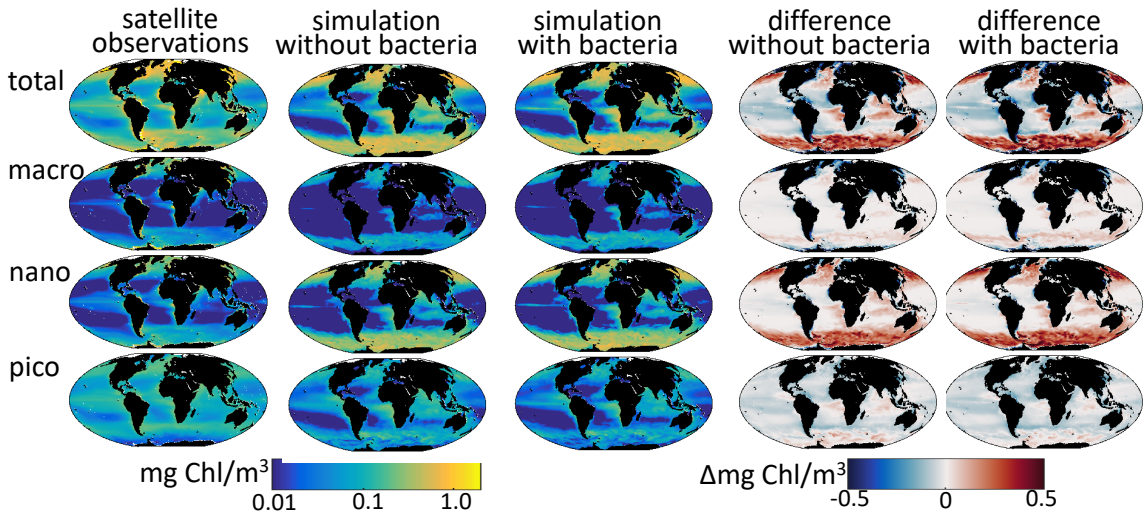

Fig. S2. Annual mean surface Chl (mg/m^3) from (left column) Satellite observations (NASA MODIS), and three-dimensional global biophysical model simulations (second column) without explicit grazing, and (third column) with explicit grazing. Left two columns show the difference between the simulations and the satellite observations (positive values indicate model over-estimates). Top row is for total Chl-a, while the lower rows the Chl-a is split into size classes based on equivalent spherical diameter (ESD): macro (>20μm), nano(2-20μm) and pico (<2μm). For the observations the size divisions from a satellite product determined from total Chl-a concentrations (8).

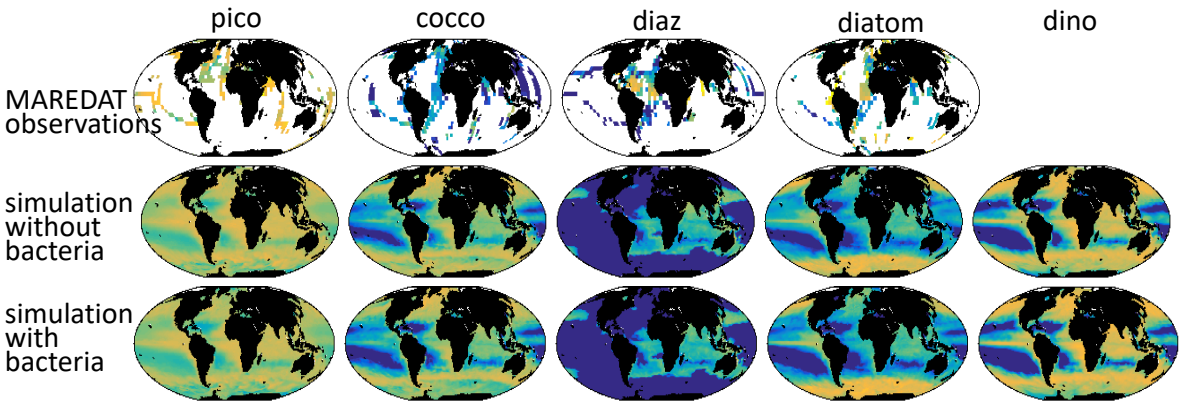

Fig. S3. Surface phytoplankton group biomass (g C/m^3) from (top row) compilation of shipboard in situ data (MAREDAT (9)), and three-dimensional global biophysical model simulations annual mean (second two) without explicit grazing, and (third crow) with explicit grazing. Columns are arranged as functional groups from pico-phytoplankton (ESD<2μm (10)), coccolithophores (11), nitrogen fixing diazotrophs (12), diatoms (13), and mixotrophic dinoflagellates. Note that MAREDAT did not collect dinoflagellate data.

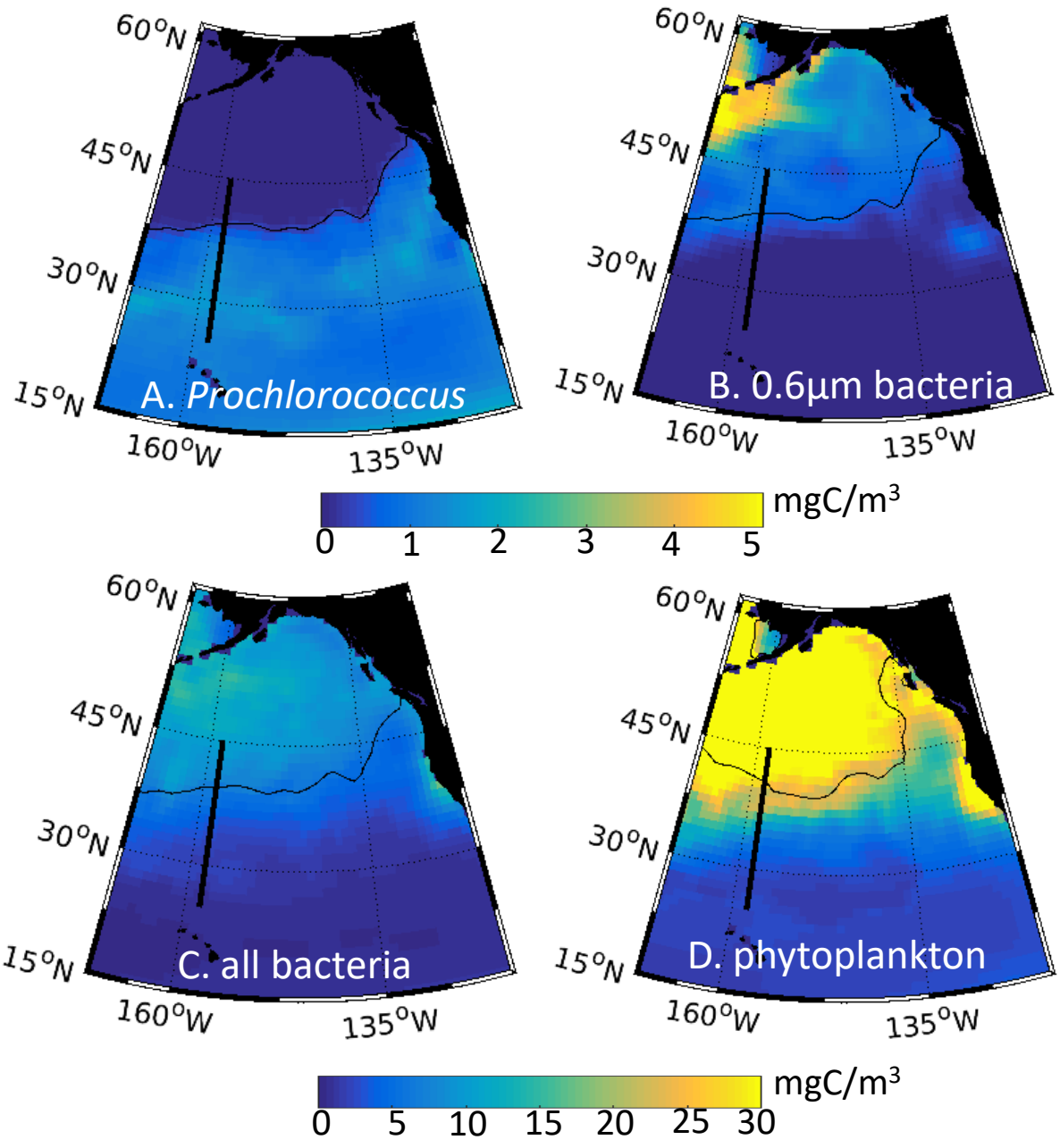

Fig. S4. Annual mean model surface biomass (mg C/m^3) for analogs of (A) $Prochlorococcus$, (B) second size class (0.6 μm ESD) heterotrophic bacteria, (C) total heterotrophic bacteria, (D) total phytoplankton. Black line indicates the collapse of the $Prochlorococcus$-anlaogs. Note that colorbar for top and bottom panels is different.

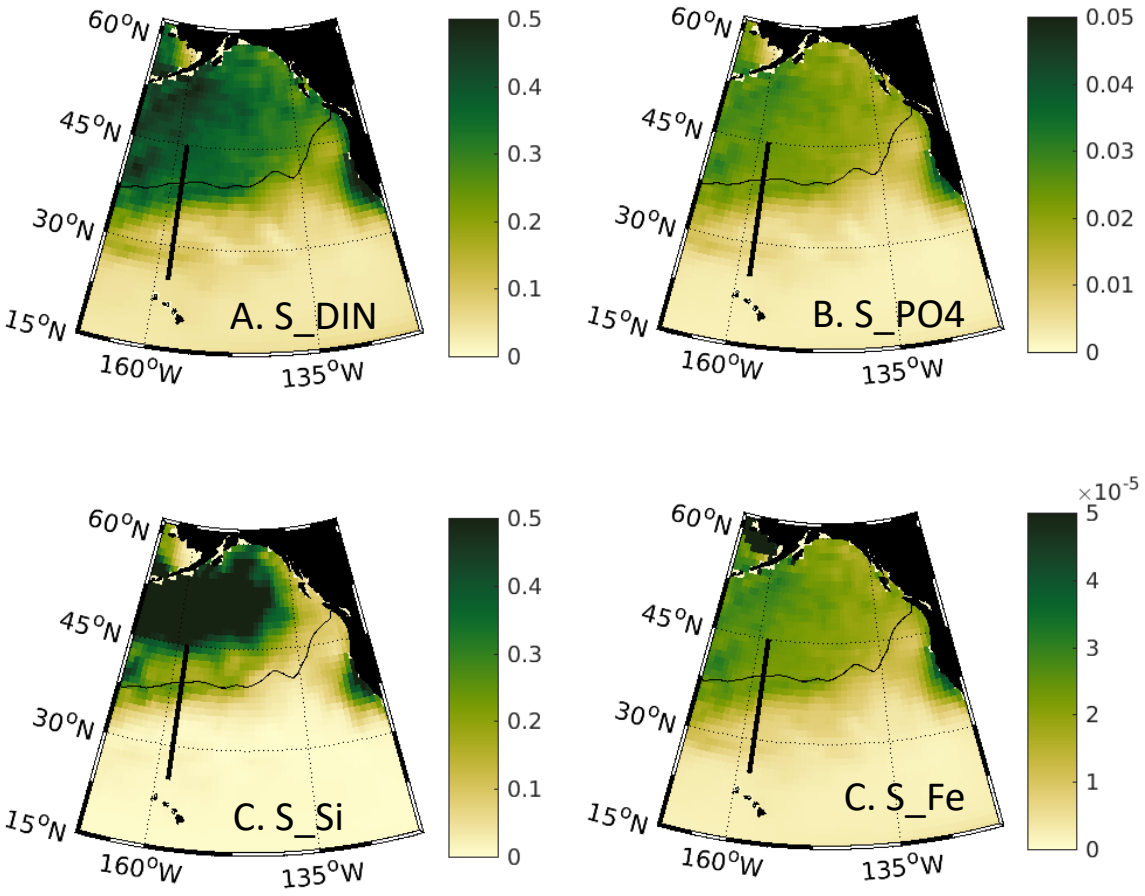

Fig. S5. Annual mean rate of supply of nutrients into the top 50m of the model ocean: (A) dissolved inorganic nitrogen (mmol N/m^3/y), (B) phosphate (mmol P/m^3/y), (C) silicic acid (mmol Si/m^3/y), (D) dissolved inorganic iron (mmol Fe/m^3/y). Black line indicates the collapse of the $Prochlorococcus$-anlaogs. Supply rate include all physical transport of the nutrient, remineralization, and in the case of iron, also aeolian dust.

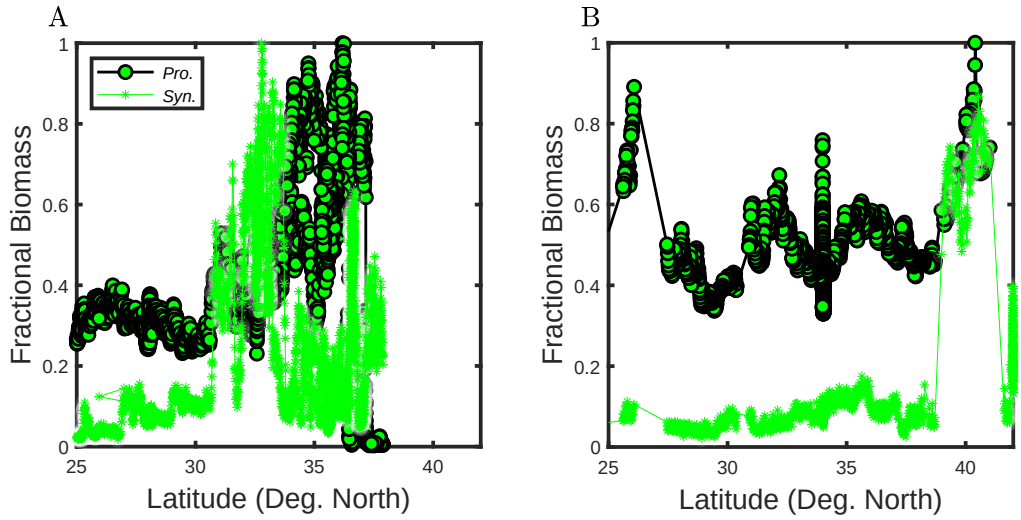

Fig. S6. Trends in $Prochlorococcus$ and $Synechococcus$ Biomass: The fractional biomass (relative to maximum value of each species along transect) of these two phytoplankton for (A) a transect in the North Pacific in April 2016 and (B) similar transect from September 2017. Cruises are the same as in Fig. 5.

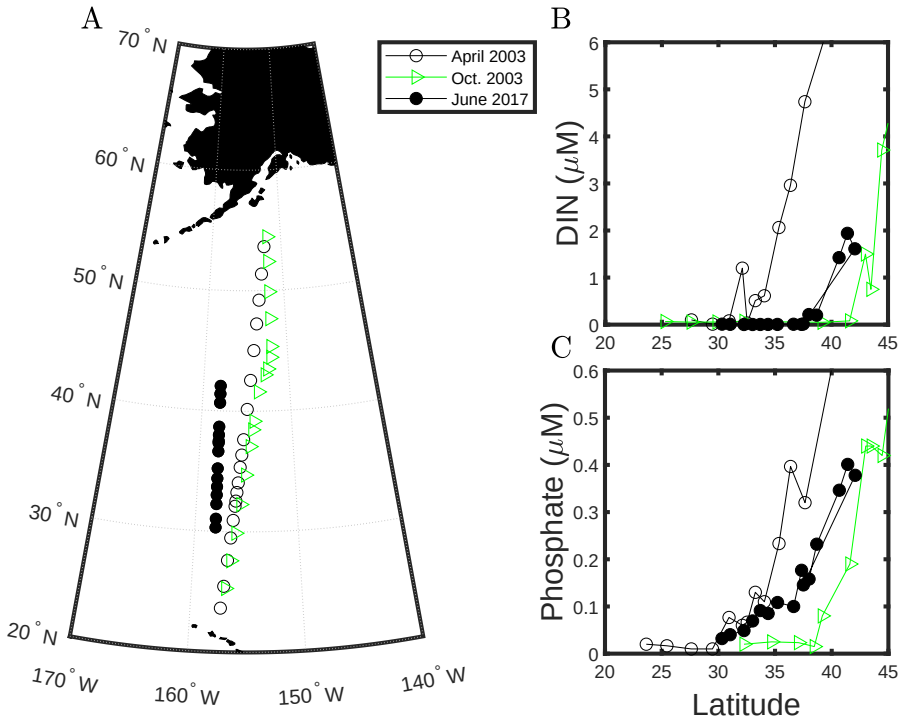

Fig. S7. Latitudinal trends in dissolved inorganic nitrogen (DIN) and phosphate for three of the cruises shown in the main text. Data for the September 2017 cruise are not available.